LETTER

ACS chemical biology

Peptide Inhibitors Targeting *Clostridium difficile* Toxins A and B

Sanofar J. Abdeen, Rebecca J. Swett, and Andrew L. Feig*

Department of Chemistry, Wayne State University, 5101 Cass Avenue, Detroit, Michigan 48202, United States

ABSTRACT *Clostridium difficile* causes severe hospital-acquired antibiotic-associated diarrhea due to the activity of two large protein toxins. Current treatments suffer from a high relapse rate and are generating resistant strains; thus new methods of dealing with these infections that target the virulence factors directly are of interest. Phage display was used to identify peptides that bind to the catalytic domain of *C. difficile* Toxin A. Library screening and subsequent quantitative binding and inhibition studies showed that several of these peptides are potent inhibitors. Fragment-based computational docking of these peptides elucidated the binding modes within the active site. These antitoxin peptides may serve as potential lead compounds to further engineer peptidomimetic inhibitors of the clostridial toxins.

C is a clinically important opportunistic pathogen and leading cause of hospital-acquired antibiotic-associated diarrhea (*1*). Over the past decade, *C. difficile* has become a growing threat worldwide (*2, 3*) due to prevalence of hypervirulent strains (*3–6*) and more recently food-borne infectivity (*7–10*). Pathogenicity of *C. difficile* derives primarily from two major toxins known as Toxin A (TcdA, 308 kDa) and Toxin B (TcdB, 270 kDa) (*11*). They are encoded within the 19.6 kb pathogenicity locus and share 45% sequence similarity (*2, 12*). Both toxins harbor four conserved regions including an N-terminal enzymatic region, a protease domain, a C-terminal receptor binding region known as CROP (C-terminal repetitive oligopeptides) and a translocation region (*11, 12*). The toxins are taken up by host cells through endocytosis but escape the endosome during acidification (*12*). Processing by the internal protease domain releases the catalytic domain to the cytosol (*13, 14*) where it irreversibly glucosylates the RhoA family of small GTPases and induces apoptosis (*13, 15*).

Current treatment involves the use of metronidazole or vancomycin (*16–18*), but antibiotic resistance is becoming a serious problem. Direct targeting of the toxins rather than the microbe itself can avoid the development of resistant strains (*19*) and thus has begun to receive significant attention. Strategies involving toxin-binding resins (*20, 21*), immunotherapy (*22, 23*), and probiotic agents (*24, 25*) are all currently under development. Structure-based glucosyltransferase inhibitors have been another area of interest in glycobiology (*26*). Recent studies have reported using UDP-mannose against *Clostridium sordellii* lethal toxin (*27*) and castanospermine for *C. difficile* TcdB (*28*). Peptides or peptidomimetics that interact with the active site of TcdA/TcdB would be another approach to combat CDAD. This mode of inhibition has precedent as it was successfully employed against anthrax toxin (*29*). This study reports a collection of peptides selected to bind the active site of TcdA and to inhibit glucosylation of Rho family GTPases.

For the initial library, the commercially available PhD-7 system (NEB) was selected. Since direct surface immobilization of target proteins can lead to partial denaturation, an affinity capture method was used, immobilizing the recombinant catalytic fragment ($rTcdA^{540}$) to Ni-NTA resin. The biopanning protocol (Figure 1, panel a) was specifically designed to identify those phage that bind $rTcdA^{540}$ within the substrate binding pocket by requiring direct competition with RhoA. To avoid selecting Ni-NTA binding sequences, the library was precleared three times to remove those phage that bound resin in the absence of $rTcdA^{540}$. This step was reiterated at the beginning of each round of selection. During the first round, bound phage were recovered nonspecifically by release with EDTA. In the next three rounds, the bound phage were eluted competitively with RhoA while increasing

***Corresponding author,**
afeig@chem.wayne.edu.

Received for review July 13, 2010 and accepted September 23, 2010.
Published online September 23, 2010
10.1021/cb100209b

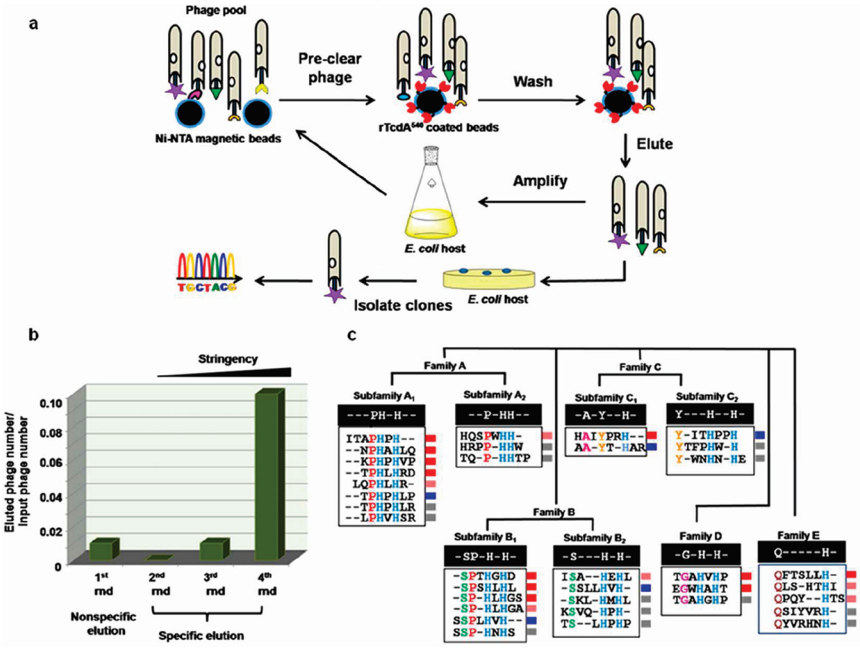

Figure 1. Overview of biopanning strategy and selection process. a) Schematic diagram of the phage display protocol. b) Histogram showing the progress of biopanning over the course of the selection process indicating the fraction of the phage recovered during each round. c) Families of peptide sequences identified from the analysis of 200 independent phage sequences and their apparent affinities. The binding affinities were obtained by a phage-based preliminary ELISA. Those marked in red exhibited binding affinities <200 nM; blue, 200−1000 nM; and gray, >1 μM.

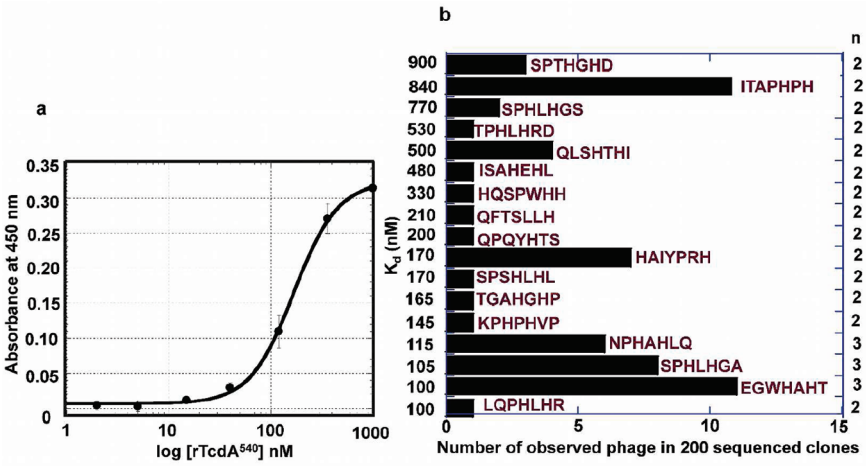

Figure 2. Binding data for phage displaying inhibitory peptides. a) Representative binding plot showing the interaction of phage HAIYPRH binding rTcdA^{540} with K_d of 170 ± 10 nM and cooperativity factor of 3. b) Histogram showing the frequency with which each of the 17 tight binding peptides were observed among the 200 phage sequenced. Peptides are ordered on the basis of their affinities for rTcdA^{540} and cooperativity values (n) are shown at the far right. All K_d values are the mean of four independent experiments.

the stringency of the washing to improve overall affinity of the surviving phage.

As shown in Figure 1, panel b, despite an equal number of phage being introduced during each round of selection, the number of eluted phage decreased in the second round. This result indicates that by switching from nonspecific to competitive elution, nonspecific peptides that survived the first round were removed from the pool. During rounds 2−4, phage recovery increased continuously, and at the end of the fourth round, 10% of all input phage were captured.

Analysis of 200 peptide sequences revealed 36 unique peptides, many of which were identified multiple times (Figure 1, panel c). These peptides were divided into five distinct families based on their sequence similarity (Families A−E) and highly structured subfamilies, suggesting that these peptides are not random but have been preferentially selected.

Individual phage were then tested in isolation to measure their affinity for TcdA. First, a rapid ELISA screen was used employing a single concentration of rTcdA^{540} (Figure 1, panel c), identifying 17 individual peptides (shown in red) with the tightest toxin binding. Hit scores reflected the binding capacities of each phage (described in detail in Methods). A quantitative ELISA assay was then used to measure affinities (K_d) for the phage-bound peptides by titrating the amount of rTcdA^{540} immobilized in each well. Overall, peptides exhibited cooperative binding with Hill coefficients of 2−3 and with K_d values ranging from mid-nanomolar to low-micromolar (Figure 2, panels a and b). In a polyvalent phage display, multiple binding events can give rise to chelate or avidity effects leading to overrepresentation of lower affinity peptides during the selection process. Since the natural substrate RhoA has poor affinity (K_M > 300 μM) to TcdA (*30*), the peptides exhibit

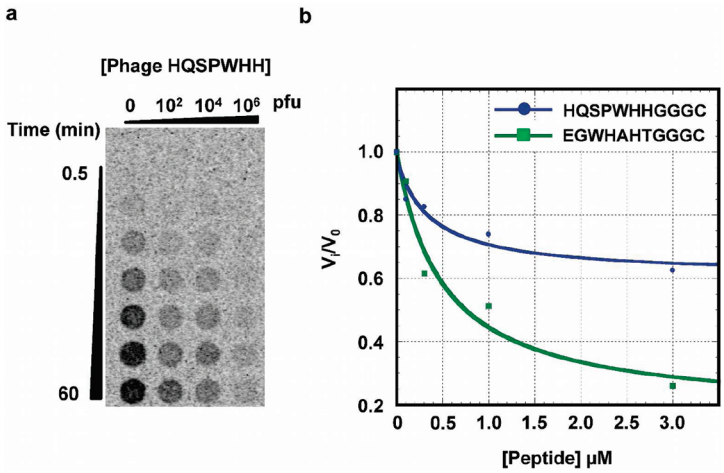

Figure 3. Inhibition of glucosyltransferase activity of rTcdA^{540}. a) Phosphorimage of an inhibition assay time course involving phage displaying the peptide HQSPWHH. Each column is an independent 60 min time course. A representative progress curve is shown in Supplementary Figure 1. b) Glucosyltransferase inhibition plot for synthetic peptides HQSPWHHGGGC and EGWHAHTGGGC showing the relative rate (v_i/v_0 where v_i is the rate in the presence of inhibitor and v_0 is the rate in the absence of inhibitor) as a function of peptide concentration.

tight binding relative to that of the natural substrate.

Two phage sequences were selected for detailed inhibition analysis. Phage displaying the peptide EGWHAHT is a tight binder from family D ($K_d \approx 100$ nM) and was among the tightest interactions from the initial screen. HQSPWHH from Family A2 binds toxin with modest affinity ($K_d \approx 330$ nM) but showed the highest affinity in computational docking studies (see below). Inhibition activity was tested using a filter plate assay (*30*). UDP-[^{14}C]-glucose, rTcdA^{540}, and phage were incubated with RhoA in glucosylation buffer. Aliquots were removed at desired time points, quenched, and applied to a protein binding membrane to capture the radiolabeled product. Control experiments in the absence of RhoA verified that the TcdA was incapable of glucosylating phage proteins (data not shown). Typical data from a kinetic time course, measured as a function of phage concentration, are shown in Figure 3, panel a and Supplementary Figure S1. Both peptides HQSPWHH and EGWHAHT effectively inhibit glucosyltransfer activity (GT) (Supplementary Table S1). Surprisingly, in the context of the phage, HQSPWHH was 100-fold more effective as an inhibitor than EGWHAHT (Supplementary Table S1), despite the fact that EGWHAHT has a tighter binding affinity. Thus, the phage that bind most tightly to TcdA are not necessarily the best glucosylation inhibitors.

Phage-based inhibition must be compared to that of the free peptides. Synthetic peptides with the sequence EGWHAHTGGGC and HQSPWHHGGGC were therefore prepared and tested for GT inhibition activity with both TcdA^{540} (Figure 3, panel b) and TcdB (Supplementary Figure 2). These data were fit to a partial competitive inhibition model to obtain the apparent K_i. Consistent with the phage-based inhibition studies, HQSPWHHGGGC had a lower K_i (300 $\pm$ 200 nM) compared to that of EGWHAHTGGGC (500 $\pm$ 200 nM), but a lower overall extent of inhibition (Supplementary Table S1). Promisingly, the peptides effectively inhibit both TcdA and TcdB in the low- to mid-nanomolar range. A nonspecific 7-mer peptide from a different phage display experiment employing the PhD-7 library showed no inhibition (data not shown).

In addition to the GT activity, TcdA and TcdB also catalyze UDP-glucose hydrolysis (GH activity) in the absence of a suitable protein substrate. Although GH activity is thought to be irrelevant *in vivo*, it is useful enzymologically to identify and characterize the properties of inhibitors. Both peptides tested effectively inhibited GH activity at low (0.5 mM) UDP-glucose concentrations (Supplementary Figure S3), and inhibition behavior was competitive with respect to UDP-glucose. The partial competitive inhibition with respect to RhoA thus results from the UDP-Glc concentrations used in the enzyme assays to ensure rapid GT activity and may be less important in a cellular context where UDP-Glc concentrations are ~100 nM (*31*).

To better understand how the peptides bind to *C. difficile* toxins, a computational approach was used. Molecular models of the selected peptides were created and flexibly docked into N-terminal catalytic domain of TcdB (*32*). The crystal structure of the N-terminal catalytic domain of TcdB was used as the catalytic domain as TcdA has not been crystallographically resolved. Both TcdA and TcdB target Rho proteins, Rac1, and Cdc42 and have identical substrate specificities. Furthermore, the catalytic domains of TcdA and TcdB exhibit 74% sequence homology (*1*), making it a suitable substitute for these studies. The docked structures were then validated using molecular dynamics under full solvation. Over a 10 ns timecourse, no major rearrangements were observed.

Peptides EGWHAHT and HQSPWHH both bind with their N-terminal residue occupying the active site (Figure 4). Binding conformations exhibit backbone coordination of the catalytic metal ion and electrostatic interactions with the highly charged active site region. HQSPWHH adopts a curled conformation (Figure 4, panel a) in order to facilitate

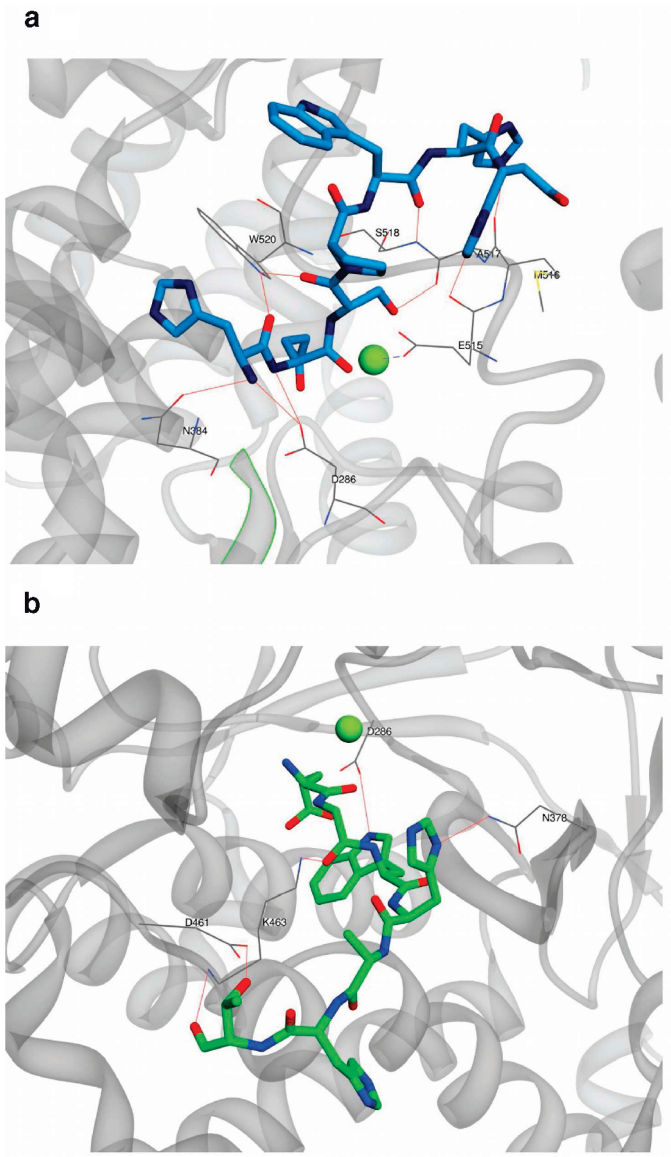

Figure 4. Binding modes of peptides HQSPWHH (blue) and EGWHAHT (green) derived from computational docking. a) HQSPWHH in the TcdB active site. b) EGWHAHT in the TcdB active site. Catalytic magnesium is indicated as a green sphere. Additional images of the binding interaction are available in the Supporting Information.

interaction of the C-terminal histidines with the charged loop region comprised of residues 513−526, a known mobile loop within the active site critical for GT activity (*33, 34*). Ser3 and Pro4 flank Trp520, blocking its availability for catalysis. Histidines 6 and 7 form close contacts with Met516 and a Arg526 respectively (Supplementary Figure S4 and Table S2). The curled conformation directs the backbone segment between the serine and the proline to the coordination sites of the magnesium (Supplementary Figure S4), while allowing the N-terminal histidine to contact a pocket comprised of an Arg273-Asp270 pair. EGWHAHT adopts an extended conformation (Figure 4, panel b) inserting His4 in a charged pocket comprised of Asn378, Lys380, and Lys463, positioning it between Trp102 and 520 of TcdB, both of which are required by the toxin for catalytic activity (*33, 34*). His6 contacts the catalytic mobile loop region between residues 514 and 520 (Supplementary Figure S5).

In summary, here we present two peptide inhibitors for TcdA and TcdB with mid-nanomolar K_i values. The computationally determined conformations of these peptides in the active site can be used to determine their potential for further functionalization. Although the protein−peptide contacts involve a large surface area, only a few of these contacts are likely to contribute the majority of the overall binding energy. With these peptides in hand and ongoing work probing their interaction with the toxins, we can use this knowledge to engineer peptide mimetics and small molecules with better *in vivo* stability and inhibitory activity to use against *C. difficile* infections.

METHODS

rTcdA^{540} Purification. All procedures with rTcdA^{540} DNA were carried out in a Biosafety Level 2 lab (BL2) following standard operating procedures. The N-terminal minimal catalytic domain of *C. difficile* Toxin A composed of residues 1−540 (rTcdA^{540}) was successfully cloned, and catalytic activity was confirmed (*30*). *E. coli* BL21 (DE3) cells (Stratagene) harboring a rTcdA^{540} plasmid was used for protein expression. Cells were lysed by sonication in 50 mM sodium phosphate, 300 mM NaCl, 10 mM imidazole, at pH 8.0, supplemented with EDTA-free complete protease inhibitor cocktail (Roche). The cell lysate was clarified by centrifugation and sterile filtered (0.22 μm filter). The protein was purified using a nickel-chelated HiTrap column (GE Healthcare) and eluted with 250 mM imidazole. It was further purified over a HiLoad 16/60 Superdex 200 gel filtration column (GE Healthcare). Size exclusion column fractions were reapplied to the nickel-chelated HiTrap column to concentrate the protein and eluted in a small volume of buffer containing 250 mM imidazole. The purified protein was dialyzed into storage buffer (50 mM HEPES-K, 100 mM KCl and 1 mM $MgCl_2$, at pH 7.5) and stored at 4 °C.

RhoA Purification. The glutathione-*S*-transferase (GST)-tagged RhoA was purified using *E. coli* Roset-

acs chemical biology

ta2 (DE3) cells (Invitrogen) harboring pGEX-2T-RhoA-GST, courtesy of the Richard A. Cerione lab (*35*). Cells were lysed by sonication in PBS, supplemented with EDTA-free complete protease inhibitor cocktail (Roche). The clarified cell lysate was loaded onto immobilized Glutathione resin (Thermo Scientific) and incubated for 1 h at 4 °C on a rotating platform. After the incubation period, the slurry was transferred to a disposable plastic column (Thermo Scientific). Bound protein was eluted in 50 mM Tris·HCl, containing 10 mM reduced glutathione at pH 8.

E. coli Rosetta2 (DE3) cells (Invitrogen) containing pET28a vector with His_6-tagged human RhoA were also utilized for protein expression (*30*). Cells were lysed by sonication in lysis buffer (50 mM HEPES, 300 mM NaCl, 1 mM $MgCl_2$ pH 8.0), supplemented with protease inhibitors. Proteins were purified using an imidazole gradient from a nickel-chelated HiTrap column.

Both the purified GST-tagged and His_6-tagged protein were dialyzed into storage buffer and stored at 4 °C.

Phage Display. M13 phage-based 7-mer linear peptide library (Ph.D-7 peptide library from New England Biolabs) was used as the initial phage display library. Magnetic Ni-NTA bead-based affinity capture was used to immobilize rTcdA^{540}. Therefore a preclearance step was performed prior to each round of panning to remove plastic and Ni^{2+} binders from the phage pool. Ni-NTA (250 μg capacity) magnetic agarose beads (QIAGEN) were washed 5 times with TBST buffer (50 mM Tris.HCl, 150 mM NaCl, 0.1% [v/v] Tween-20, pH 7.5). TBST buffer containing 10^{10} pfu mL^{-1} of the phage library was incubated with washed Ni-NTA magnetic agarose beads at RT for 1 h with continuous rotation. The supernatant of this solution provided the precleared phage pool. For target immobilization, 20 μL of washed Ni-NTA magnetic agarose beads (50 μg capacity) were coated for 1 h at RT with 100 μg of purified His-tagged rTcdA^{540} with continuous rotation. After the incubation period, unbound toxin was washed away with storage buffer. The precleared phage pool was added to the rTcdA^{540} coated Ni-NTA beads and incubated at RT for 1 h with continuous rotation. Unbound phage were removed by washing 20 times with 200 μL of TBST buffer. Four rounds of elution were performed under the following conditions: TBST buffer supplemented with 50 mM EDTA for round 1, 25 μg of purified glutathione-*S*-transferase-tagged RhoA in round 2, and 50 μg of purified GST-tagged RhoA for rounds 3 and 4.

At the end of each round of selection, eluted phage were amplified in *E. coli* ER2738 cells (NEB) and phage were counted. After the fourth round, 200 phage colonies were selected randomly. Phage DNA was purified using the manufacturers protocol (NEB) and sequenced (Beckman-Coulter CEQ8000 sequencer).

Preliminary ELISA To Identify rTcdA^{540} Binding Peptides. A 96-well flat-bottom black assay plate (Fisher) was incubated with TBS (50 mM Tris·HCl, 150 mM NaCl, pH 7.5) buffer containing 10^{10} pfu from each of 36 phage colonies overnight at 4 °C. (Note: all colonies were plated in duplicate, allowing one well to serve as a negative control.) After the incubation period, the wells were washed 6 times with TBS and then blocked with 2% bovine serum albumin (Sigma) in TBS for 2 h at RT. Wells were then washed 6 times with TBS. Storage buffer (negative control) or storage buffer supplemented with 2 μM rTcdA^{540} was added to each well. The plate was incubated at RT for 1 h with shaking and then washed 3 times with TBS buffer. To each well 1 μg mL^{-1} His Probe-HRP [a nickel (Ni^{2+}) activated derivative of horseradish peroxidase (Thermo Scientific)] was added and incubated at RT for 1 h. Wells were washed 4 times with TBS. To each well was added 200 μL of a 1:1 mixture of Luminol/Enhancer Solution with Stable Peroxide Solution (Thermo Scientific), and after 5 min chemiluminesence was measured on a luminometer (Tecan GENios Plus multi label reader). Sample readings were compared to their corresponding negative control to obtain a hit score using eq where A_0 is the chemiluminescence of the sample and B_0 is the intensity of the negative control.

$$\text{hit score} = \frac{\log(A_0 - B_0)}{\log B_0} \qquad (1)$$

Quantitative Phage-rTcdA^{540} Binding Assay. Purified rTcdA^{540} (2−1000 nM in storage buffer) was coated overnight at 4 °C to 96-well flat-bottom transparent assay plates (Fisher). After the coating step, unbound toxin was removed, and wells were washed with storage buffer. Plates were blocked for 2 h at RT with a solution of 2% nonfat dry milk in storage buffer and then washed again. Approximately 40 μL of solution containing 1 × 10^{10} phage was added to wells and incubated for 3 h at RT with shaking. After washing 6 times with storage buffer, the plates were incubated for an additional 1 h with anti-M13 monoclonal antibody coupled to horseradish peroxidase (GE healthcare) (1:10,000 dilution into storage buffer). Unbound antibodies were removed, and the wells were washed 10 times with storage buffer. The enzymatic activity was assayed by addition of 1 Step Turbo TMB-ELISA (Thermo Scientific). The reaction was terminated with 100 μL of 1 M H_2SO_4. Color intensity was quantified at 450 nm using a Tecan GENios Plus multi label plate reader and compared to control reactions using milk-coated wells. Data were plotted as the mean ± SD of four independent experiments. Binding data were fit using nonlinear least-squares analysis (Kaleidagraph, Synergy Software) to a cooperative binding model (*36*).

Phage-Based Glucosyl Transfer Inhibition Assay. Glucosyltransferase activity in the presence or absence of inhibitory phage was measured by preincubating 2 nM rTcdA^{540} with 10^{10} pfu phage for 1 h at 37 °C. Reaction was initiated by addition of preincubated toxin-phage mixture to glucosylation buffer (50 mM HEPES-K, 100 mM KCl, 2 mM $MgCl_2$, 2 mM MnCl2, pH 7.5) containing 2 μM RhoA, 15 μM UDP-glucose (Sigma) and 15 μM UDP-[^{14}C]-glucose (Perkin-Elmer). At appropriate time points (0.5, 2, 5, 10, 20, 40, 60 min) 8-μL aliquots were removed and quenched into 40 μL of 10 mM EDTA at pH 8.0. Quenched sample points were loaded onto a Biodyne-B high-protein binding 96-well filter plate (Nunc) and aspirated into a collection plate in a MultiScreen Vacuum Manifold (Millipore). The filter membrane was washed extensively with wash buffer (50 mM HEPES-K, 100 mM KCl, pH 7.5), dried, and imaged overnight in a phosphorimage cassette. A Typhoon phosphorimager (GE Healthcare) and ImageQuant software were used to quantify the pixel intensities.

Pixel intensities were converted to moles of [^{14}C]-glucosylated RhoA by using a standard curve (*30*). A GT reaction containing 20 μM RhoA, 163 nM rTcdA^{540}, and 30 μM UDP-[^{14}C]-glucose (Perkin-Elmer) was incubated at 37 °C for 5 h to achieve quantitative modification of RhoA. The reaction mixture was then dialyzed using a 3500 MWCO Slide-A-Lyzer Cassette (Pierce) to remove all unincorporated label. Serially diluted dialyzed reaction mixture was applied to Biodyne-B high-protein binding 96-well filter plate (Nunc), while duplicate samples were analyzed by liquid scintillation counter (Beckman Coulter). Radioactivity was then directly related to the amount of ^{14}C-labeled RhoA retained on the filter membrane, which provides the conversion factor to moles of ^{14}C retained on the membrane. The standard curve membrane is exposed on the same PI plate with all experimental data to account for differential exposure.

Apparent inhibition constants (K_i) were obtained by fitting the ratio of initial rate of the GT assay, in the presence (v_i) and absence (v_0) of peptide using nonlinear linear least-squares analysis to a reversible partial competitive inhibition model (*37*), eq , where I is the phage or peptide inhibitor concentration, K_M is the Michaelis constant for RhoA, K_i is the inhibition constant, S is the substrate concentration (RhoA), and X_0 is the coefficient of maximum inhibition under the experimental conditions.

$$\frac{v_i}{v_0} = \frac{K_M}{K_M\left(1 + \frac{I}{K_i}\right) + S} + X_0 \qquad (2)$$

Peptide Inhibition of Glucosyltransferase and Glucosylhydrolase Activity. Synthetic peptides EGWHAHTGGGC and HQSPWHHGGGC with C-terminal amide-modification were purchased from American Peptide Company, Inc. Sunnyvale, CA. Peptides were purified by reverse-phase HPLC over a C18 column (Beckman Coulter)], using a gradient of 0−100% acetonitrile containing 0.1% trifluoroacetic acid and monitored by UV absorption. After purification, the peptide was lyophilized and redissolved in water. The identity of each product was confirmed by electrospray mass spectrometry.

GT inhibition assays contained 10 μM RhoA, 15 μM UDP-glucose (Sigma), and 15 μM UDP-[^{14}C]-glucose (Perkin-Elmer) in glucosylation buffer as described above, as well as 0−3000 nM peptide. Reactions were initiated by addition of 2 nM rTcdA^{540} or TcdB (courtesy of Prof. Hanping Feng (*38*)). K_i values were obtained by fitting the data to a partial competitive inhibition model as described for the phage-based GT inhibition assays.

GH activity was measured using a coupled enzyme assay. UDP released during the hydrolysis is coupled to the oxidation of NADH using pyruvate kinase and lactate dehydrogenase (*39*). The reaction was carried out using an Agilent 8453 UV−vis spectrophotometer equipped with a circulating water bath to maintain the temperature at 37 °C. Reaction was monitored by adding 200 nM $rTcdA^{540}$ to glucosylation buffer supplemented with UDP-glucose, 0.2 mM NADH, 1 mM phosphoenolpyruvate (PEP), 3 units of pyruvate kinase, and 6 units of lactate dehydrogenase. The initial GH rate was measured at 0.5 mM UDP-glucose (standard saturation conditions) in the absence or presence of inhibitory peptides (10 nM for HQSPWHHGGGC or 1 μM for EGWHAHTGGGC). UDP-glucose was varied from 0.5 to 13.5 mM to monitor the effect of increased substrate concentration on the inhibition behavior. The relative rate (V_i/V_0) was calculated by ratio of initial rate of the GH assay, in the presence and absence of peptide.

Peptide Docking. Molecular models of selected peptides were built using Spartan '02 (*40*), minimizing at the AM1 level of theory. Models were saved in Sybyl mol2 format and catenated into a library for docking. Flexible docking was performed using FlexX 3.1.0 (*41*). Crystal structure 2BVL (*32*) was retrieved from the RCSB database for use as the docking receptor. Crystallographic phasing markers and counterions were removed, retaining crystallographic water molecules. The active site for docking was defined by 20 Å spheres around each atom of the crystallographically observed UDP. The crystallographic catalytic manganese was replaced with a magnesium ion for ease of calculation. A docking pharmacophore with two optional constraints was constructed utilizing the two octahedral coordination sites of the magnesium occupied by the crystallographic UDP molecule. Dockings performed without the use of a pharmacophore resulted in identical conformations. Water molecules within the active site were included in the docking, designated as fully rotatable and displaceable. Dockings were ranked using the FlexX internal scoring protocol (*42*). Results were viewed, and all images were generated using the UCSF Chimera visualization program (*43*) version1.4.1. The docked structures were then simulated for 10 ns to determine the stability of the docked conformation. The complete protein/peptide complex was solvated and ionized to 0.5 mM NaCl and simulated using the CHARMM27 force field under NAMD (*1*) on the WSU Grid supercomputer. A time step of 1 fs was used, periodic boundary conditions were applied, and Langevin dynamics were utilized to maintain constant temperature at 300 K. A scaled cutoff was employed in the calculation of the long-range electrostatics. Activity of the simulation was monitored by Generalized Masked Delaunay analysis using TimeScapes (*44*) as well as visual inspection.

Acknowledgment: The authors wish to thank Andres Cisneros and members of the Chow Lab including P. N. Asare-Okai for providing nonspecific peptides for inhibition studies and helpful discussions on this work. We also thank Hanping Feng (Tufts University School of Medicine) for providing rTcdB for these studies. We acknowledge the generous financial support of Wayne State University, Office of the Vice President for Research, and the Department of Chemistry.

Supporting Information Available: This material is available free of charge *via* the Internet at http://pubs.acs.org.

REFERENCES

1. Voth, D. E., and Ballard, J. D. (2005) *Clostridium difficile* toxins: mechanism of action and role in disease, *Clin. Microbiol. Rev. 18*, 247–263.
2. Gould, C. V., and McDonald, L. C. (2008) Bench-to-bedside review: *Clostridium difficile* colitis, *Crit. Care 12*, 203.
3. Wamy, M., Pepin, J., Fang, A., Killgore, G., Thompson, A., Brazier, J., Frost, E., and McDonald, L. C. (2005) Toxin production by an emerging strain of *Clostridium difficile* associated with outbreaks of severe disease in North America and Europe, *Lancet 366*, 1079–1084.
4. Loo, V. G., Poirier, L., Miller, M. A., Oughton, M., Libman, M. D., Michaud, S., Bourgault, A. M., Nguyen, T., Frenette, C., Kelly, M., Vibien, A., Brassard, P., Fenn, S., Dewar, K., Hudson, T. J., Horn, R., Rene, P., Monczak, Y., and Dascal, A. (2005) A predominantly clonal multi-institutional outbreak of *Clostridium difficile*-associated diarrhea with high morbidity and mortality, *N. Engl. J. Med. 353*, 2442–2449.
5. Goorhuis, A., Van der Kooi, T., Vaessen, N., Dekker, F. W., Van den Berg, R., Harmanus, C., van den Hof, S., Notermans, D. W., and Kuijper, E. J. (2007) Spread and epidemiology of *Clostridium difficile* polymerase chain reaction ribotype 027/toxinotype III in The Netherlands, *Clin. Infect. Dis. 45*, 695–703.
6. Goorhuis, A., Bakker, D., Corver, J., Debast, S. B., Harmanus, C., Notermans, D. W., Bergwerff, A. A., Dekker, F. W., and Kuijper, E. J. (2008) Emergence of *Clostridium difficile* infection due to a new hypervirulent strain, polymerase chain reaction ribotype 078, *Clin. Infect. Dis. 47*, 1162–1170.
7. Weese, J. S. (2010) *Clostridium difficile* in food−innocent bystander or serious threat? *Clin Microbiol Infect 16*, 3–10.
8. Bakri, M. M., Brown, D. J., Butcher, J. P., and Sutherland, A. D. (2009) *Clostridium difficile* in ready-to-eat salads, Scotland, *Emerging Infect. Dis. 15*, 817–818.
9. Jobstl, M., Heuberger, S., Indra, A., Nepf, R., Kofer, J., and Wagner, M. (2010) *Clostridium difficile* in raw products of animal origin, *Int. J. Food Microbiol. 138*, 172–175.
10. Rupnik, M., Widmer, A., Zimmermann, O., Eckert, C., and Barbut, F. (2008) *Clostridium difficile* toxinotype V, ribotype 078, in animals and humans, *J. Clin. Microbiol. 46*, 2146.
11. Just, I., and Gerhard, R. (2004) Large clostridial cytotoxins, *Rev. Physiol. Biochem. Pharmacol. 152*, 23–47.
12. von Eichel-Streiber, C., Laufenberg-Feldmann, R., Sartingen, S., Schulze, J., and Sauerborn, M. (1992) Comparative sequence analysis of the *Clostridium difficile* toxins A and B, *Mol. Gen. Genet. 233*, 260–268.
13. Rupnik, M., Pabst, S., von Eichel-Streiber, C., Urlaub, H., and Soling, H. D. (2005) Characterization of the cleavage site and function of resulting cleavage fragments after limited proteolysis of *Clostridium difficile* toxin B (TcdB) by host cells, *Microbiology 151*, 199–208.
14. Pruitt, R. N., Chagot, B., Cover, M., Chazin, W. J., Spiller, B., and Lacy, D. B. (2009) Structure-function analysis of inositol hexakisphosphate-induced autoprocessing in *Clostridium difficile* toxin A, *J. Biol. Chem. 284*, 21934–21940.
15. Just, I., Selzer, J., Wilm, M., von Eichel-Streiber, C., Mann, M., and Aktories, K. (1995) Glucosylation of Rho proteins by *Clostridium difficile* toxin B, *Nature 375*, 500–503.
16. Al-Nassir, W. N., Sethi, A. K., Nerandzic, M. M., Bobulsky, G. S., Jump, R. L., and Donskey, C. J. (2008) Comparison of clinical and microbiological response to treatment of *Clostridium difficile*-associated disease with metronidazole and vancomycin, *Clin. Infect. Dis. 47*, 56–62.
17. Shetler, K., Nieuwenhuis, R., Wren, S. M., and Triadafilopoulos, G. (2001) Decompressive colonoscopy with intracolonic vancomycin administration for the treatment of severe pseudomembranous colitis, *Surg. Endosc. 15*, 653–659.
18. Pepin, J., Valiquette, L., Gagnon, S., Routhier, S., and Brazeau, I. (2007) Outcomes of *Clostridium difficile*-associated disease treated with metronidazole or vancomycin before and after the emergence of NAP1/027, *Am. J. Gastroenterol. 102*, 2781–2788.
19. Clatworthy, A. E., Pierson, E., and Hung, D. T. (2007) Targeting virulence: a new paradigm for antimicrobial therapy, *Nat. Chem. Bio.l 3*, 541–548.
20. Baines, S. D., Freeman, J., and Wilcox, M. H. (2009) Tolevamer is not efficacious in the neutralization of cytotoxin in a human gut model of *Clostridium difficile* infection, *Antimicrob. Agents Chemother. 53*, 2202–2204.
21. Peppe, J., Porzio, A., and Davidson, D. M. (2008) A new formulation of tolevamer, a novel nonantibiotic polymer, is safe and well-tolerated in healthy volunteers: a randomized phase I trial, *Br. J. Clin. Pharmacol. 66*, 102–109.
22. Hassoun, A., and Ibrahim, F. (2007) Use of intravenous immunoglobulin for the treatment of severe *Clostridium difficile* colitis, *Am. J Geriatr. Pharmacother. 5*, 48–51.
23. Sanchez-Hurtado, K., Corretge, M., Mutlu, E., McIlhagger, R., Starr, J. M., and Poxton, I. R. (2008) Systemic antibody response to *Clostridium difficile* in colonized patients with and without symptoms and matched controls, *J. Med. Microbiol. 57*, 717–724.
24. Karpa, K. D. (2007) Probiotics for *Clostridium difficile* diarrhea: putting it into perspective, *Ann. Pharmacother. 41*, 1284–1287.
25. Segarra-Newnham, M. (2007) Probiotics for *Clostridium difficile*-associated diarrhea: focus on *Lactobacillus rhamnosus* GG and *Saccharomyces boulardii*, *Ann. Pharmacother. 41*, 1212–1221.

26. Gloster, T. M., Meloncelli, P., Stick, R. V., Zechel, D., Vasella, A., and Davies, G. J. (2007) Glycosidase inhibition: an assessment of the binding of 18 putative transition-state mimics, *J. Am. Chem. Soc. 129*, 2345–2354.
27. Humeau, Y., Popoff, M. R., Kojima, H., Doussau, F., and Poulain, B. (2002) Rac GTPase plays an essential role in exocytosis by controlling the fusion competence of release sites, *J. Neurosci. 22*, 7968–7981.
28. Jank, T., Ziegler, M. O., Schulz, G. E., and Aktories, K. (2008) Inhibition of the glucosyltransferase activity of clostridial Rho/Ras-glucosylating toxins by castanospermine, *FEBS Lett. 582*, 2277–2282.
29. Basha, S., Rai, P., Poon, V., Saraph, A., Gujraty, K., Go, M. Y., Sadacharan, S., Frost, M., Mogridge, J., and Kane, R. S. (2006) Polyvalent inhibitors of anthrax toxin that target host receptors, *Proc. Natl. Acad. Sci. U.S.A. 103*, 13509–13513.
30. Kerzmann, A. (2009) Ph.D. Thesis. Mechanistic Analysis of Clostridium difficile Toxin A. Indiana University, Bloomington, IN.
31. Laughlin, M. R., Petit, W. A., Jr., Dizon, J. M., Shulman, R. G., and Barrett, E. J. (1988) NMR measurements of in vivo myocardial glycogen metabolism, *J. Biol. Chem. 263*, 2285–2291.
32. Reinert, D. J., Jank, T., Aktories, K., and Schulz, G. E. (2005) Structural basis for the function of *Clostridium difficile* toxin B, *J. Mol. Biol. 351*, 973–981.
33. Belyi, Y., and Aktories, K. (1800) (2010) Bacterial toxin and effector glycosyltransferases, *Biochim. Biophys. Acta 134*, 143.
34. Ziegler, M. O., Jank, T., Aktories, K., and Schulz, G. E. (2008) Conformational changes and reaction of clostridial glycosylating toxins, *J. Mol. Biol. 377*, 1346–1356.
35. Hart, M. J., Eva, A., Zangrilli, D., Aaronson, S. A., Evans, T., Cerione, R. A., and Zheng, Y. (1994) Cellular transformation and guanine nucleotide exchange activity are catalyzed by a common domain on the dbl oncogene product, *J. Biol. Chem. 269*, 62–65.
36. Narindrasorasak, S., Lowery, D., Gonzalez-DeWhitt, P., Poorman, R. A., Greenberg, B., and Kisilevsky, R. (1991) High affinity interactions between the Alzheimer's beta-amyloid precursor proteins and the basement membrane form of heparan sulfate proteoglycan, *J. Biol. Chem. 266*, 12878–12883.
37. Ritchie, D. W. (2005) High-order analytic translation matrix elements for real-space six-dimensional polar Fourier correlations, *J. Appl. Crystallogr. 38*, 808–818.
38. Yang, G., Zhou, B., Wang, J., He, X., Sun, X., Nie, W., Tzipori, S., and Feng, H. (2008) Expression of recombinant *Clostridium difficile* toxin A and B in *Bacillus megaterium*, *BMC Microbiol. 8*, 192.
39. Gosselin, S., Alhussaini, M., Streiff, M. B., Takabayashi, K., and Palcic, M. M. (1994) A continuous spectrophotometric assay for glycosyltransferases, *Anal. Biochem. 220*, 92–97.
40. Spartan '02. Wavefunction, Inc. 18041 Von Karman Ave. Suite 370, Irvine, CA 92612 .
41. Schellhammer, I., and Rarey, M. (2004) FlexX-Scan: fast, structure-based virtual screening, *Proteins 57*, 504–517.
42. Gohlke, H., Hendlich, M., and Klebe, G. (2000) Knowledge-based scoring function to predict protein-ligand interactions, *J. Mol. Biol. 295*, 337–356.
43. Pettersen, E. F., Goddard, T. D., Huang, C. C., Couch, G. S., Greenblatt, D. M., Meng, E. C., and Ferrin, T. E. (2004) UCSF Chimera—a visualization system for exploratory research and analysis, *J. Comput. Chem. 25*, 1605–1612.
44. Wriggers, S., Stafford, K. A., Shan, Y., Piana, S., Maragakis, P., Lindorff-Larsen, K., Miller, P. J., Gullingsrud, J., Rendleman, C. A., Eastwood, M. P., Dror, R. O., and Shaw, D. E. (2009) Automated event detection and activity monitoring in long time-scale molecular dynamics, *J. Chem. Theory Comput. 5*, 2595–2605.